Effect of the Met344His Mutation on the Conformational Dynamics of Bovine β-1,4-Galactosyltransferase: Crystal Structure of the Met344His Mutant in Complex with Chitobiose[†,‡,§]

Boopathy Ramakrishnan,[⊥,||] Elizabeth Boeggeman,[⊥,||] and Pradman K. Qasba*[,⊥]

Structural Glycobiology Section, Laboratory of Experimental and Computational Biology, and Basic Research Program, SAIC-Frederick, Inc., Center for Cancer Research, National Cancer Institute, Frederick, Maryland 21702-1201

Received May 17, 2004; Revised Manuscript Received June 30, 2004

ABSTRACT: β-1,4-Galactosyltransferase (β4Gal-T1) in the presence of manganese ion transfers galactose from UDP-galactose (UDP-Gal) to *N*-acetylglucosamine (GlcNAc) that is either free or linked to an oligosaccharide. Crystallographic studies on bovine β4Gal-T1 have shown that the primary metal binding site is located in the hinge region of a long flexible loop, which upon Mn^{2+} and UDP-Gal binding changes from an open to a closed conformation. This conformational change creates an oligosaccharide binding site in the enzyme. Neither UDP nor UDP analogues efficiently induce these conformational changes in the wild-type enzyme, thereby restricting the structural analysis of the acceptor binding site. The binding of Mn^{2+} involves an uncommon coordination to the Sδ atom of Met344; when it is mutated to His, the mutant M344H, in the presence of Mn^{2+} and UDP-hexanolamine, readily changes to a closed conformation, facilitating the structural analysis of the enzyme bound with an oligosaccharide acceptor. Although the mutant M344H loses 98% of its Mn^{2+}-dependent activity, it exhibits 25% of its activity in the presence of Mg^{2+}. The crystal structures of M344H-Gal-T1 in complex with either UDP-Gal·Mn^{2+} or UDP-Gal·Mg^{2+}, determined at 2.3 Å resolution, show that the mutant enzyme in these complexes is in a closed conformation, and the coordination stereochemistry of Mg^{2+} is quite similar to that of Mn^{2+}. Although either Mn^{2+} or Mg^{2+}, together with UDP-Gal, binds and changes the conformation of the M344H mutant to the closed one, it is the Mg^{2+} complex that engages efficiently in catalyses. Thus, this property enabled us to crystallize the M344H mutant for the first time with the acceptor substrate chitobiose in the presence of UDP-hexanolamine and Mn^{2+}. The crystal structure determined at 2.3 Å resolution reveals that the GlcNAc residue at the nonreducing end of chitobiose makes extensive hydrophobic interactions with the highly conserved Tyr286 residue.

β-1,4-Galactosyltransferases (β4Gal-T,[1] EC 2.4.1.90/38) are a Golgi resident, type II membrane-bound family of enzymes (β4Gal-T1−T7) that transfer galactose (Gal) in the presence of manganese ion, from UDP-Gal to *N*-acetylglucosamine (GlcNAc), either free or bound to an oligosaccharide of a glycoprotein or a glycolipid (*1*−*3*). The family members exhibit a high level of sequence identity in their catalytic domains (*4*, *5*). Although they have the same donor sugar specificity, many of these are expected to transfer Gal to different oligosaccharides containing GlcNAc at their nonreducing end. Recent crystallographic studies on β4Gal-T1 have provided detailed information about the structure and function of the enzyme (*6*−*11*). These studies have shown that upon substrate binding β4Gal-T1 undergoes conformational changes that involve two loops: a short loop, residues 313−315 containing Trp314, and a longer loop comprising residues 345−365. The conformational changes of these two loops are highly coordinated. Trp314 in the small loop plays a crucial role in the conformational state of the long loop, in the binding of the substrates, and in the catalytic mechanism of the enzyme (*7*, *12*, *13*). In the unbound state (open conformation), the side chain of Trp is exposed to the solvent (*6*, *13*), and the conformation of the long loop is such that the UDP-Gal and the metal binding sites are exposed. Once the substrate binds, the side chain of Trp314 moves into the catalytic pocket to lock the sugar

[†] This project has been funded in part with federal funds from the National Cancer Institute, National Institutes of Health, under Contract N01-C0-12400.

[‡] The content of this publication does not necessarily reflect the view or policies of the Department of Health and Human Services, nor does mention of trade names, commercial products, or organizations imply endorsement by the U.S. Government.

[§] Protein Data Bank accession numbers for the crystal structures are as follows: M344H-Gal-T1-Gal+, PDB 1TVY, PDB 1TW1; M344H-Gal-T1+, PDB 1TW5.

* To whom correspondence should be addressed: Structural Glycobiology Section, LECB, CCR, NCI-Frederick, Building 469, Room 221, Frederick, MD 21702. E-mail: qasba@helix.nih.gov. Phone: (301) 846-1934. Fax: (301) 846-7149.

[⊥] Structural Glycobiology Section.

[||] Basic Research Program.

[1] Abbreviations: β4Gal-T1, β1,4-galactosyltransferase; GlcNAc, *N*-acetylglucosamine; UDP-Gal, uridine 5′-diphosphogalactose; UDP, uridine 5′-diphosphate; UDPH/UDP-hexanolamine, uridine 5′-diphosphohexanolamine; SDS, sodium dodecyl sulfate; WT, wild type; Mes, 2-morpholinoethanesulfonic acid; chitobiose, 4-*O*-(2-acetamido-2-deoxy-β-D-glucosyl)-2-acetamido-2-deoxy-D-glucose.

10.1021/bi049007+
Published on Web 09/14/2004

nucleotide in its binding site. Simultaneously, the long loop changes to its closed conformation, masking the sugar nucleotide binding site (*7*, *11*, *13*). Furthermore, this conformational change in the long flexible loop repositions the amino acid residues at the N-terminal region, creating a metal ion binding site, and at the C-terminal region, creating an oligosaccharide-binding cavity that is also a protein−protein interaction site for α-lactalbumin (LA) (*6*, *9*, *11*). LA is a mammary gland-specific protein that modulates the acceptor specificity of the enzyme toward glucose (*14*). LA binds at the extended sugar binding site, present only in the closed conformer of β4Gal-T1, leaving the monosaccharide binding site of the enzyme available for the binding of Glc or GlcNAc. Since LA competes with the oligosaccharide for binding to the extended sugar binding site (*15*, *16*), it is not possible to crystallize β4Gal-T1 in the presence of LA with a bound oligosaccharide acceptor. The wild-type enzyme also does not crystallize in the presence of UDP or UDP-hexanolamine, Mn^{2+}, and oligosaccharides, thereby restricting our structural or biochemical studies on the interactions of oligosaccharides with β4Gal-T1. It has previously been shown that the sugar moiety of the sugar nucleotide is essential for efficiently inducing a conformational change in β4Gal-T1 (*17*).

Of the six ligands that coordinate Mn^{2+}, three are from β4Gal-T1: Asp254, Met344, and His347 (*7*, *11*, *18*). Residues Met344 and His347, separated by the hinge residue Ile345, are at the N-terminal region of the long flexible loop. The complete metal binding site is created only after His347 has moved during the conformational change to coordinate with the metal ion. To influence the conformational dynamics of the long loop, we mutated the residues of the metal binding region. Mutation of Asp254 or His347 results in either a total or large loss of the enzyme activity, while mutation of Met344 to Ala or Gln results in an only moderate loss of activity (*18*). These studies suggested that Met344 coordination with Mn^{2+} might not be essential for the catalytic activity. To further understand the role of Met344 in the metal binding and conformational change in β4Gal-T1, in the study presented here we mutated it to His and found that the mutant M344H-Gal-T1, in the presence of Mn^{2+}, has only 1.5% of the wild-type enzyme activity. On the other hand, the mutant M344H-Gal-T1 exhibits 25% of its catalytic activity in the presence of an alkali metal ion, Mg^{2+}. In contrast, Mg^{2+} does not activate the wild-type enzyme. Although metal ions Mg^{2+} and Mn^{2+} bind to the mutant M344H-Gal-T1, their enzyme kinetics are different, indicating that the residue at position 344 and the appropriate metal ion play an important role in the conformational dynamics of the long loop in the catalytic mechanism of β4Gal-T1.

In the presence of Mn^{2+} and UDP-Gal, or UDP-hexanolamine, the mutant M344H-Gal-T1 crystallizes in the closed conformation. This has enabled us to crystallize the mutant in complex with chitobiose, in the presence of Mn^{2+} and UDP-hexanolamine. In the crystal structure of the complex with chitobiose, the GlcNAc residue at the reducing end of the disaccharide binds to β4Gal-T1 in a manner similar to that of GlcNAc bound in the LS−GlcNAc complex (*7*, *11*). The second nonreducing end GlcNAc residue of the disaccharide forms extensive hydrophobic interactions with the highly conserved Tyr286 residue.

MATERIALS AND METHODS

Site-directed mutagenesis was performed using the PCR method. Construction of the mutants was carried out using plasmid pEGT-d129 as the template. This plasmid contains a *Bam*HI−*Eco*RI fragment inserted into a pET23a vector, encoding residues 130−402 of bovine β4Gal-T1 (*19*), and has a Cys342Thr mutation. The mutation primers corresponding to the upper DNA strand are as follows: 5′-ATCGGGAAG*ACGCGT***CAC**ATCCGCCACTCGAGAGAC-3′ (M344H) and 5′-ATCGGGAAG*ACGCGT***GAG**ATCC-GCCACTCGAGAGAC-3′ (M344E). The restriction site *Mlu*I is shown in italics and the mutation codon in bold type. Typically, the Gal-T1 DNA fragment between *Mlu*I and *Eco*RI was PCR-amplified using the terminal cloning primer and the mutagenesis primer. The fragment was cut with restriction enzymes *Mlu*I and *Eco*RI and ligated with the precut plasmid pEGT-129 DNA with the same enzymes. Mutants were screened for the presence of full Gal-T1 DNA, and then sequenced. The positive clones were transformed into BL21(DE3) pLysS cells as described previously (*8*). The mutant proteins were expressed and purified according to the published method (*8*).

β4Gal-T Enzyme Assays. The protein concentrations were measured using the Bio-Rad protein assay kit, based on the Bradford method, and further verified on SDS−PAGE gels using standard protein concentration markers. An *in vitro* assay procedure for Gal-T1 has been reported previously (*8*). The activities were measured using UDP-Gal as a sugar nucleotide donor, and GlcNAc (βGlcNAc1−4GlcNAc and β-benzyl-GlcNAc) as the acceptor sugar. For the specific activity measurements, a 100 μL incubation mixture containing 25 mM GlcNAc, 5 mM $MnCl_2$ or $MgCl_2$, 20 mM Tris-HCl (pH 8.0), 500 μM UDP-Gal, 500 ng of M344H-Gal-T1 or 30 ng of C342T-Gal-T1, and 0.5 μCi of [^{3}H]UDP-Gal was used for each Gal-T reaction. The incubation was carried out at 30 °C for 15 min. The reaction was terminated by adding 200 μL of cold water, and the mixture was passed through a 0.5 mL bed volume column of AG 1-X8 cation resin (Bio-Rad) to remove any unreacted [^{3}H]UDP-Gal. The column was washed successively with 300, 400, and 500 μL of cold water, and the column flow-through was diluted with Biosafe scintillation fluid; radioactivity was measured with a Beckman counter. A reaction without the acceptor sugar was used as a control. A concentration of $ZnCl_2$ or $CoCl_2$ of only 0.1 mM was used whenever Zn^{2+} or Co^{2+} was used during the enzyme assay.

Determining the Kinetic Constants. The enzyme activation data, at various concentrations of Mg^{2+}, were fitted to an equation describing binding of metal to a high-affinity site (K_{d1}) to generate an enzyme form with a low k_{cat} (V_1) and to a second, lower-affinity site (K_{d2}) to generate a form with a higher k_{cat} (V_2) (*18*):

$$v = \frac{[Mg](V_1K_{d2} + V_2[Mg])}{K_{d1}K_{d2} + K_{d2}[Mg] + [Mg][Mg]}$$

The true K_m of the donor (K_A) and of the acceptor (K_B), the dissociation constant of the donor (K_{ia}), and k_{cat} were obtained using two-substrate analyses and the primary plots of at least five concentrations of the donor (UDP-Gal) and five concentrations of the acceptor, and the correspond-

Table 1: Statistics for Data Collection and Refinement

	M344H-Gal-T1·UDP-Gal·Mn^{2+}	M344H-Gal-T1·UDP-Gal·Mg^{2+}	M344H-Gal-T1·UDPH·Mn^{2+}·chitobiose
data collection wavelength (Å)	0.9807	0.9807	1.5418
cell dimensions (*a*, *b*, *c*) (Å)	50.4, 91.8, 142.5	50.0, 91.5, 142.8	50.4, 92.6, 143.4
resolution range (Å)	40−2.3	40−2.3	40−2.3
space group	$P2_12_12_1$	$P2_12_12_1$	$P2_12_12_1$
no. of observations	139305	83034	136286
no. of unique reflections	29843	29702	31209
R_{symm} (%) (outermost shell)[a]	4.8 (17)	7.2 (47)	8.3 (39)
completeness (%) (outermost shell)[a]	98.5 (98)	98.6 (99)	99 (97)
$I/\sigma(I)$ (outermost shell)[a]	15.3 (2.4)	12.3 (2.1)	16.2 (3.0)
R_{cryst} [$I > 0$, $I > 2\sigma(I)$]	19.6, 18.8	19.6, 18.3	19.6, 18.7
R_{free}[b] [$I > 0$, $I > 2\sigma(I)$]	25, 24	26, 24	26, 23
deviations from ideality			
bond lengths (Å)	0.01	0.01	0.011
bond angles (deg)	1.7	1.8	1.7
Ramachandran plot			
core region (%)	88.1	86.2	86.8
allowed region (%)	11.9	12.8	13.2

[a] Shell being 2.38−2.3 Å. [b] R_{free} is equal to R_{cryst} for a randomly selected 10% of reflections, not used in refinement.

ing secondary plots of the intercepts and slopes. Initial rate conditions were linear with respect to time. A suitable range of donor and acceptor concentrations was chosen, which allowed accurate Michaelis−Menten constants to be derived. The data were also analyzed for a general two-substrate system using the following equations (*20*) with EnzFitter, a Biosoft nonlinear curve fitting program for Windows:

$$v = \frac{V_{max}[A][B]}{K_{ia}K_B + K_B[A] + K_A[B] + [A][B]} \quad (1)$$

$$v = \frac{V_{max}[A][B]}{K_B[A] + K_A[B] + [A][B]} \quad (2)$$

where v is the initial velocity and the rate equation for a sequential, symmetrical, initial velocity pattern associated with eq 1, an ordered or random equilibrium mechanism in which substrate A dissociates well from the ECS complex with a dissociation constant of K_{ia}. Equation 2 is for an asymmetric initial velocity pattern for a double-displacement, or "ping-pong", mechanism. The kinetic parameters K_A, K_B, K_{ia}, and V_{max} were obtained from the fitted curves using the rate equations given above. The graphical method and EnzFitter gave very similar kinetic parameters. In the β4Gal-T assay, the maximum substrate concentrations used for UDP-Gal and GlcNAc were 0.2 and 25 mM, respectively (which are 3-fold higher than their K_m values).

Crystal Structure Determination. The mutant M344H-Gal-T1 was cocrystallized in the presence of UDP-Gal and $MnCl_2$ or $MgCl_2$. The crystals were grown at room temperature by the hanging drop method, using 30 mg/mL mutant protein, 17 mM UDP-Gal, and 17 mM $MgCl_2$ or $MnCl_2$, with the precipitant containing 10% (v/v) dioxane, 100 mM Mes-NaOH buffer (pH 6.5), and 2.0 M ammonium sulfate. Complete three-dimensional X-ray diffraction data were collected at beam line X9B (National Synchrotron Light Source, Brookhaven National Laboratory, Upton, NY), using a Quantum-4 ccd detector. The frames were processed using HKL2000 (*21*). The crystal and data collection parameters are listed in Table 1. Since the crystals were isomorphous with the C342T-Gal-T1·UDP-Gal·Mn^{2+} complex crystals, that structure was used as a starting model without any substrate. An initial model containing Ala at position 344 was used. After initial refinement, the difference Fourier electron density maps not only confirmed the mutation but also revealed the UDP-Gal and Mn^{2+} or Mg^{2+} bound to the enzyme. These features were included in the further refinement. All the refinements were carried out with CNS version 1.0 (*22*). The final refinement statistics are given in Table 1. All figures were drawn using MOLSCRIPT (*23*), BOBSCRIPT (*24*), and Grasp (*25*). The coordinates have been deposited in the Protein Data Bank.

Identification of the Metal Ions in the Crystal Structures. Since these crystals can be grown only if metal ions are used in the crystallization, it is safe to say that the metal ion used in the crystallization is the one observed in the crystal structure. Furthermore, a Mn^{2+} and a Mg^{2+} in the crystal structure can be differentiated by their relative electron density, compared to the phosphate groups to which they are bound. In the case of the Mg^{2+}-bound structure, the difference Fourier electron density of the phosphate groups (16σ) is stronger than that found at the Mg^{2+} position (12σ), while in the case of a Mn^{2+}-bound structure, the difference Fourier electron density at the Mn^{2+} position (24σ) is stronger than that of the phosphate groups (17σ). Furthermore, in these crystal structures, the average isotropic temperature factors for the phosphate group and the bound metal ion are comparable; they are 27 and 25 Å^2, respectively, for the Mg^{2+}-bound structure and 17 and 14 Å^2, respectively, for the Mn^{2+}-bound structure.

Crystallization and Determina tion of the Structure of the M344H-Gal-T1·UDPH·Mn^{2+}·Chitobiose Complex. The crystals of the complex were grown by hanging drop methods using the mother liquid containing 20 mg/mL protein, 2 mM chitobiose, 17 mM $MnCl_2$, and UDP-hexanolamine, with the precipitant containing 1.8 M ammonium sulfate, 100 mM Mes-NaOH buffer (pH 6.5), and 10% dioxane. The three-dimensional X-ray diffraction data were collected at 100 K, using an in-house X-ray generator equipped with a mar345 image plate. The data collection and the refinement statistics are given in Table 1. The data processing and the structure solution were carried out in a manner similar to the methods described above. In addition to finding a chitobiose molecule

Table 2: Catalytic Activity (picomoles per minute per nanogram) in the Presence of Various Metal Ions[a]

metal	wild-type β4Gal-T1	M344H	M344E	M344A	M344S	M344Q
Mn	5.35	0.13[c]	0.32	4.16	1.97	1.91
Co	0.41[b]	0.02	0.24	0.61[b]	0.41	0.80[b]
Zn	1.42	0.08	0.27	0.64	0.40	0.71
Mg	0	1.42	0	0	0	0
Ca	0	0.06	0.01	0	0	0
Sr	0	0.01	0.02	0	0	0

[a] All assays were carried out at 500 μM UDP-Gal, 25 mM GlcNAc, and 5 mM metal ion, except for Co^{2+} and Zn^{2+}, which were used at concentrations of 0.1 mM. [b] At 200 μM UDP-Gal, 25 mM GlcNAc, and 0.1 mM Co^{2+}, the specific activities of the wild type and mutants M344A and M344Q are 0.65, 0.55, and 0.4 pmol min^{-1} ng^{-1}, respectively. [c] M344H was assessed at 3 mM GlcNAc since, at higher concentrations, its catalytic activity is inhibited in the presence of Mn^{2+}.

in the active site of the M344H-Gal-T1 molecule, we found an additional chitobiose molecule away from the active site, wedged between two protein molecules.

RESULTS AND DISCUSSION

M344-Gal-T1 Mutants Exhibit Broad Metal Ion Specificity. Previous studies have shown that ions of alkaline earth metals, such as Mg^{2+}, Ca^{2+}, or Sr^{2+}, do not activate wild-type β4Gal-T1 because they do not bind to the primary metal binding site of the enzyme (*3*, *18*) (Table 2). Various Met344 mutants, some of them generated in a previous study (*18*), were tested for their catalytic activity in the presence of several metal ions, including alkaline earth metals. Their metal ion activation specificities differed from that of wild-type β4Gal-T1 (Table 2). Among these mutations, the substitution of Met344 with His reduces the Mn^{2+}- and Zn^{2+}-dependent activity by 98%, but the mutant exhibits Mg^{2+}-dependent activity that is nearly one-fourth of the Mn^{2+}-dependent activity of the wild-type enzyme. The fact that the wild type, which has a Met residue at position 344, can be activated, in addition to Mn^{2+} by the transition metals Co^{2+} and Zn^{2+}, suggests the participation of the side chain Sδ atom of the Met residue in the metal coordination. On the other hand, when a His residue is present at position 344, even alkali earth metal ions can bind in the primary metal ion binding site, giving higher activities with Mg^{2+} (Table 2).

Although the mutant M344H-Gal-T1 has only ~2% activity in the presence of Mn^{2+}, its activation curve is similar to that of the wild type in the presence of Mn^{2+} (Figure 1a,b). The observation that the activation of the wild type by metal ions is a sigmoidal curve has been interpreted as involving two metal binding sites of the enzyme: one with high affinity (K_{d1}), which is associated with low velocity, and the other with low affinity (K_{d2}), which is associated with high velocity (*3*, *18*). The values of the dissociation constant (K_d) for Mn^{2+} of the mutant are quite different from that of the wild type (Table 3). The K_{d1} of Mn^{2+} for the mutant is 25-fold lower than that of the wild-type enzyme, suggesting that the Mn^{2+} binds tightly to the primary metal binding site of the mutant. However, the K_{d2} for the mutant is 100-fold higher that that of the wild type, indicating that Mn^{2+} binds weakly to the second metal binding site of the mutant. The activation curve with Mg^{2+} for the mutant is also sigmoidal (inset) and strikingly similar to that of the wild-type enzyme with Mn^{2+}

Table 3: Kinetic Parameters of the Substrates[a]

ligand	parameter	wild-type β4Gal-T1 with Mn^{2+}	M344H-Gal-T1 with Mn^{2+}	M344H-Gal-T1 with Mg^{2+}
metal ion	K_{d1} (mM)	0.030(4)	0.0014(10)	0.16(8)
	K_{d2} (mM)	0.40(9)	45(10)	6.2(3)
UDP-Gal	V_{max} (pmol min^{-1} ng^{-1})	6.4(4)	0.170(5)	2.6(1)
	k_{cat} (s^{-1})	3.6	0.097	1.44
	K_{ia}	0	0	0
	K_A (μM)	95(6)	7(2)	512(24)
	k_{cat}/K_A (s^{-1} μM^{-1})	0.04	0.015	0.003
GlcNAc	K_B (mM)	10(1)	0.75(6)	25(3)
	k_{cat}/K_B (s^{-1} mM^{-1})	0.36	0.13	0.058

[a] The K_{d1} and K_{d2} values for the metal ions were derived from Figure 1. Standard deviations are given in the parentheses to their least significant decimal point.

(Figure 1a,b). The sigmoidal velocity curve for the M344H-Gal-T1 mutant with the Mg^{2+} is also suggestive of two metal binding sites, with Mg^{2+} binding not only to the first site but also to the second metal binding site. The K_d values for the binding of Mg^{2+} to sites I and II are 100- and 7-fold higher, respectively, than those for binding of Mn^{2+} to the same mutant (Table 3), indicating that Mg^{2+} compared to Mn^{2+} binds weakly to the primary binding site of the mutant.

Kinetic Parameters of the Donor and Acceptor Substrates for M344H-Gal-T1 in the Presence of Mg^{2+}. Similar to those for the wild-type enzyme with the Mn^{2+} (*26*), the double-substrate kinetic data for the mutant in the presence of Mn^{2+} and Mg^{2+} fit best to a rate equation that lacks a K_{ia} term, the dissociation constant of the UDP-Gal−metal−enzyme complex (eq 2). It describes an asymmetric initial velocity pattern associated with a sequential, or ping-pong, mechanism in which the donor substrate does not dissociate from the enzyme−substrate complex. In the presence of Mn^{2+}, the true K_m of the mutant for both the substrates, the donor UDP-Gal (K_A) and the acceptor (K_B), is nearly 13-fold reduced compared to that of the wild type, indicating that in the presence of Mn^{2+} the substrates bind strongly to the mutant. However, in the presence of Mg^{2+}, the true K_m values of the donor and acceptor for the mutant are nearly 5- and 2-fold higher, respectively, than that of wild-type β4Gal-T1 in the presence of Mn^{2+} (Table 3). Although the catalytic efficiency with respect to the donor and acceptor of the mutant in the presence of Mg^{2+}, compared to that of the wild-type enzyme with Mn^{2+}, has decreased by orders of magnitude of ~13 and ~6, respectively, the turnover number, the k_{cat} of the mutant, is reduced by only 60%. The smaller effect on k_{cat} than on k_{cat}/K_m reflects the fact that mutation (Met344 to His344) and metal substitution (Mn^{2+} to Mg^{2+}) weaken both ground state and transition state binding, but the effect on ground state binding is greater as reflected in the poorer K_m values. To determine if there are minor differences in the coordination geometry of the Mg^{2+} in the mutant compared with that of Mn^{2+} in the wild-type enzyme, which might explain the differences in the ground state binding and poorer K_m values, we determined the crystal structure of M344H-Gal-T1 in complex with UDP-Gal in the presence of either Mn^{2+} or Mg^{2+} and compared the structure with the wild type·UDP-Gal·metal complex.

Crystal Structure of the Mutant M344H-Gal-T1 in the Presence of Mn^{2+} and Mg^{2+}. The M344H-Gal-T1 mutant crystallizes readily in the presence of UDP-Gal with either

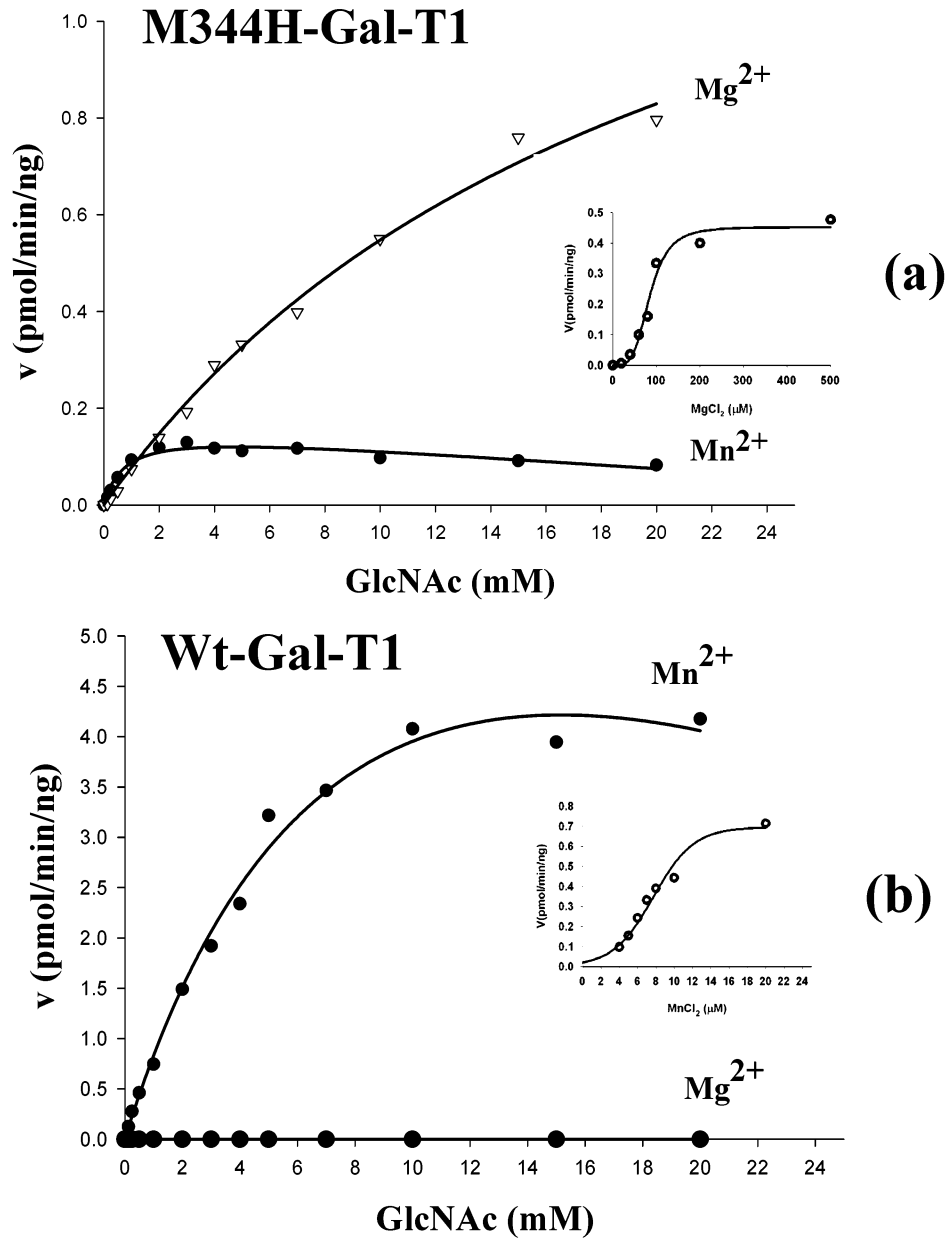

FIGURE 1: Enzyme activity with increasing concentrations of the acceptor GlcNAc for the M344H-Gal-T1 mutant (a) and for the wild type (b) in the presence of either Mn^{2+} or Mg^{2+}. Higher GlcNAc concentrations in the presence of Mn^{2+} inhibit the catalytic activity of the mutant M344H-Gal-T1, whereas such an effect was not observed with Mg^{2+}. In the wild-type enzyme, with Met at position 344, the enzyme activity is high when Mn^{2+} is used as a metal ion. When Met344 is substituted with His, the mutant exhibits high activity in the presence of Mg^{2+}. Thus, there seems to be a relationship between the residue and the choice of metal ion for the maximum catalytic activity of the enzyme. Insets show the sigmoidal metal ion activation curves. At lower concentrations of Mg^{2+}, the activation curve of the M344H-Gal-T1 mutant is sigmoidal (inset in panel a), as is the wild-type enzyme activation at lower concentrations of Mn^{2+} (inset in panel b), indicating the presence of two metal ion binding sites in both the mutant and wild type. Mg^{2+} also binds to the second binding site in the mutant.

$MnCl_2$ or $MgCl_2$. On the other hand, wild-type β4Gal-T1 crystallizes only in the presence of UDP-Gal and $MnCl_2$, but not in the presence of $MgCl_2$. Inclusion of metal ion in the crystallization droplet was essential for obtaining the crystal. We determined the crystal structure of the mutant M344H-Gal-T1 in complex with UDP-Gal and Mn^{2+} or Mg^{2+} (Table 1). The three-dimensional crystal structures of these complexes are quite similar. The β4Gal-T1 mutant proteins were found in the closed conformation (Figure 2a), similar to the wild-type complex with UDP-Gal·Mn^{2+} (PDB entry 1O0R) (*10*, *11*). The rms deviations between these structures and the closed structure of wild-type β4Gal-T1 vary between 0.5 and 0.6 Å on the Cα atoms, indicating that neither the mutation nor the binding of Mg^{2+} caused any significant change in the structure. In the crystal structure of the M344H-Gal-T1·UDP-Gal·Mg^{2+} complex, the metal nucleotide complex can be located clearly (Figure 2b). In these structures, the metal ions exhibit six similar coordination bonds with comparable bond distances (Table 4). Interestingly, the stereochemistry of the Mg^{2+} coordination is quite similar to that of the Mn^{2+} (Table 4). As before, the second metal ion could not be located in these studies.

A comparison of the crystal structures of M344H-Gal-T1·UDP-Gal·metal complexes (Figure 2b,c) shows that the presence of the Mg^{2+} has not perturbed the interactions between the UDP-Gal and the protein molecule, the interac-

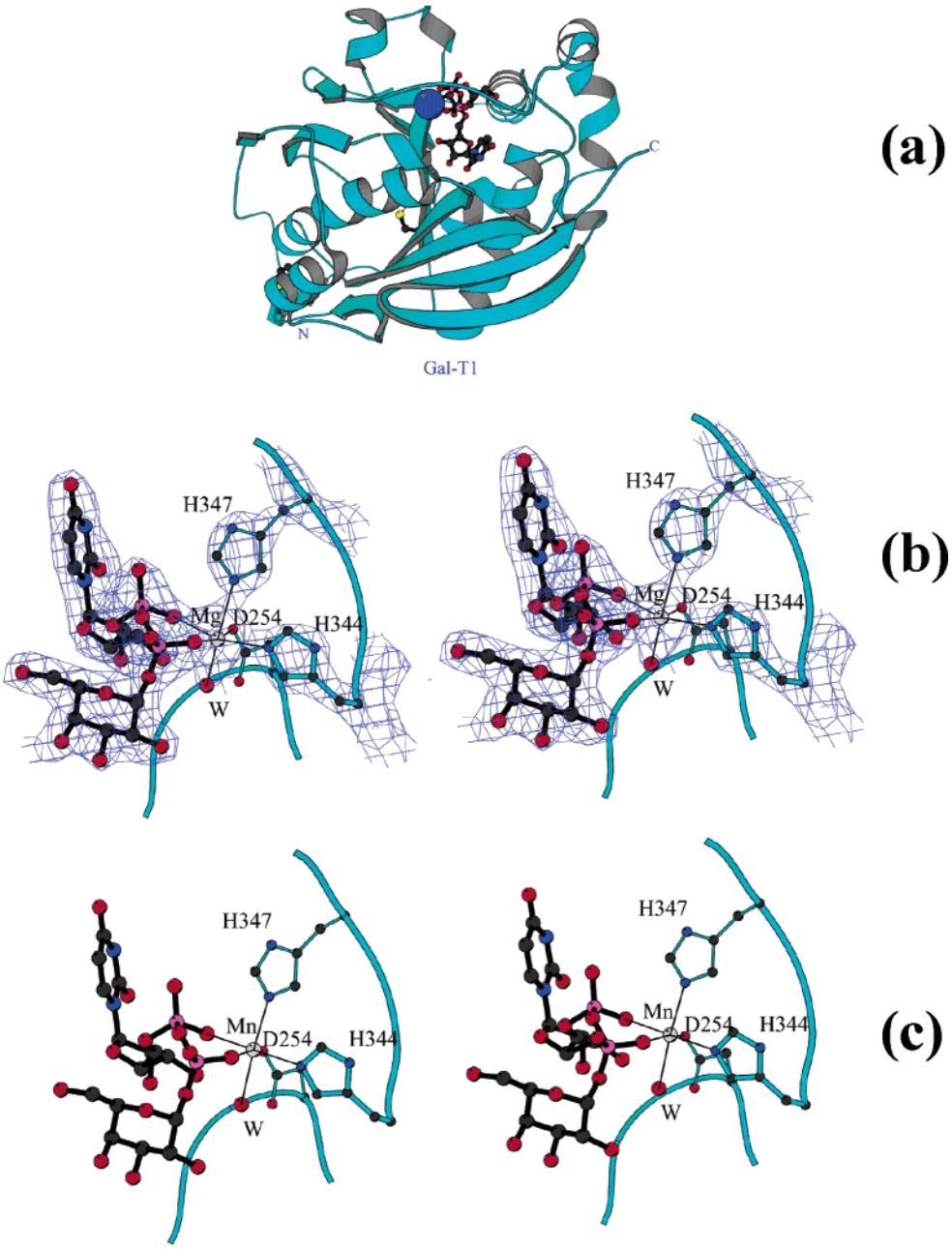

FIGURE 2: (a) Overall crystal structure of the M344H-Gal-T1 mutant, in the presence of UDP-Gal and Mg^{2+}. The metal ion is shown as a blue sphere and the UDP-Gal molecule as a ball-and-stick model. (b) Stereoview of the final electron density maps contoured at the 1.5σ level around the UDP-Gal molecule and Mg^{2+} in the crystal structure of the M344H-Gal-T1·UDP-Gal·Mg^{2+} complex. The coordination of the magnesium ion is quite similar to that of the manganese ion, which includes the sixth coordination with a water molecule. The coordination distances between the H344 residue and the Mg^{2+} are shorter than the corresponding coordination bond between Met344 and the Mn^{2+} in the wild type (*7*, *11*), indicating that even Mg^{2+} exhibits stronger binding to the M344H-Gal-T1 mutant. W represents a water molecule. (c) Binding of UDP-Gal·Mn^{2+} to the M344H-Gal-T1 mutant. The Mn^{2+} coordination is quite similar to that of the wild-type enzyme. However, the coordination bond between His344 and Mn^{2+} is stronger than the corresponding bond between M344 and Mn^{2+} in the wild-type enzyme (*7*, *11*).

tions being similar to those found in the crystal structure of the wild-type protein, β4Gal-T1, in complex with UDP-Gal·Mn^{2+} (PDB entry 1O0R) (*10*, *11*) However, the coordination distance between the Nϵ2 atom of His344 and the metal ion is shorter (2.2−2.5 Å) than the corresponding coordination distance found for the sulfur atom of Met344 in the wild type (2.7 Å). This indicates that the presence of a His residue at position 344 strengthens the binding of the metal ion to the enzyme, consistent with the K_{d1} values for Mn^{2+} observed with the mutant and the wild type (Table 3). Even though the coordination geometry of the Mn^{2+} and Mg^{2+} bound to the M344H-Gal-T1 mutant is very similar, the higher affinity toward transition metal ion Mn^{2+} (Table 3; $K_{d1} = 1.3$ μM) over an alkali earth metal ion Mg^{2+} ($K_{d1} = 160$ μM) by the His residue could hinder the formation of the enzyme transition state complex during catalysis. The observed reduced enzyme activity for the M344H-Gal-T1 mutant in the presence of Mn^{2+} compared to that of the wild type or Met344Ala mutant is suggestive of that. Besides this effect, the role of the metal ion in determining the ability of the long loop to undergo the required open to closed, and back to open, conformation change during the catalytic cycle

Table 4: Metal Ion Coordination Distances (angstroms)

	Mn^{2+} in M344H-Gal-T1·UDP-Gal·Mn^{2+}		Mg^{2+} in M344H-Gal-T1·UDP-Gal·Mg^{2+}		Mn^{2+} in wild-type Gal-T1·UDP-Gal·Mn^{2+}
coordination residue	molecule 1	molecule 2	molecule 1	molecule 2	average value
P(α)−O	2.4	2.1	2.1	1.9	2.1
P(β)−O	2.1	2.4	2.3	2.2	2.3
water	2.3	2.3	2.0	2.2	2.2
D254	2.3	2.3	2.2	2.2	2.2
H347	2.3	2.2	2.2	2.1	2.3
residue 344	2.2	2.2	2.5	2.2	2.7

seems to play an important role in determining the kinetics turnover number (k_{cat}).

Effect of the Acceptor Concentration on the Catalytic Activity of M344H-Gal-T1. In the presence of Mn^{2+}, an inhibition of the catalytic activity of the M344H-Gal-T1 mutant was observed at GlcNAc concentrations of 2−5 mM (Figure 3a), whereas much higher GlcNAc concentrations (20−25 mM) were necessary to inhibit the catalytic activity of the wild-type enzyme (Figure 3b). The inhibition of the M344H-Gal-T1 mutant with higher concentrations of the acceptor is independent of the concentration of Mn^{2+} used in the assay (Figure 3a), while in the wild type, low concentrations of metal have no effect on acceptor inhibition (Figure 3b). Acceptors with higher affinity such as chitobiose (βGlcNAc1−4GlcNAc) and β-benzyl-GlcNAc inhibit the catalytic activity of the M344H-Gal-T1 mutant at very low concentrations much more strongly than GlcNAc does (Figure 3c). On the other hand, in the presence of Mg^{2+}, under the same conditions, these acceptors do not inhibit the catalytic activity of the M344H-Gal-T1 mutant, indicating that the acceptor substrate inhibition is metal ion-dependent. Inhibition at high acceptor concentrations has been shown as noncompetitive with respect to both Mn^{2+} and UDP (*27*), and it is the result of a dead-end enzyme·Mn^{2+}·UDP·acceptor complex in the product release phase of the reaction (*15*). This indicates that during the catalytic cycle, the mutant is in the closed conformation in the presence of Mn^{2+} and UDP and is readily stabilized by the acceptor compared to the wild-type enzyme. This is consistent with a 13-fold reduction in the K_m for GlcNAc of the mutant M344H-Gal-T1, in the presence of Mn^{2+} compared to that of the wild type (Table 3). There is also a 37-fold reduction in the k_{cat} of the M344H-Gal-T1 mutant, which is related to the transition state complex and measures a 3-fold decrease in the catalytic efficiency (k_{cat}/K_B) compared to that of the wild-type enzyme. Since the acceptor binds to only the closed conformation, and UDP alone cannot cause an efficient conformational change from the open to the closed conformation (*17*), both the sugar acceptor and the metal ion seem to play important roles in the conformational changes in the mutant. This property seems to enable us to crystallize the M344H-Gal-T1 mutant with the disaccharide acceptor, chitobiose, in the presence of Mn^{2+} and UDP-hexanolamine (see below).

Structure-Based Explanation for the Role of Metal Ion in the Conformational Dynamics of M344H-Gal-T1. During the catalytic cycle, upon metal ion and UDP-Gal binding, β4Gal-T1 undergoes a conformational change, from an open to a closed structure. This creates the acceptor-binding site of the enzyme. After catalysis and release of the product disaccharide or oligosaccharide, the closed conformation reverts to the open conformation, exposing the UDP and metal ion to the solvent environment for their release, and a new round of the catalytic cycle follows. The primary metal binding site is situated in the hinge region of the long loop, where the metal binding residues, Met344 and His347, flank the hinge residue, Ile345 (Figure 4). In the open conformation, the metal ion coordinates with Asp254 and Met344 in β4Gal-T1. His347 coordinates with the metal ion only when β4Gal-T1 is in the closed conformation (*7*). Asp254 and His347 are strong metal ligands, while the coordination with Met344 is weak; thus, the product UDP and Mn^{2+} are easily released after the catalytic event. The manganese ion binds to the mutant M344H-Gal-T1 20-fold tighter than to the wild-type enzyme (Table 3; $K_{d1} = 1.3$ μM). Thus, in the product release phase, the release of UDP and Mn^{2+} may be delayed by keeping the enzyme in the closed conformation and facilitating the binding of the sugar acceptor with the formation of a dead-end molecule. This explains a strong inhibition of the Mn^{2+}-dependent catalytic activity of the M344H mutant at low concentrations of various sugar acceptors compared to the wild-type enzyme. This is further evident in the fact that the M344H-Gal-T1 mutant readily crystallizes in the presence of UDP-hexanolamine (UDPH), chitobiose, and Mn^{2+} in the closed conformation, while the wild type has not so far crystallized under similar conditions. Furthermore, magnesium binds weakly to the mutant M344H-Gal-T1 with a dissociation constant (K_{d1}) that is 100-fold higher than the K_{d1} for binding of manganese to the mutant. This allows the M344H-Gal-T1 mutant to undergo an efficient conformational change in the presence of Mg^{2+}, with the release of a final product thus exhibiting no inhibition at low substrate acceptor concentrations.

Crystal Structure of the M344-Gal-T1·UDPH·Mn^{2+}·Chitobiose Complex. In the crystal structure, there are two M344H-Gal-T1 molecules in the asymmetric unit, and they are found in the closed conformation. As expected, one molecule each of Mn^{2+}, UDP-hexanolamine, and chitobiose are bound to each protein molecule. The overall rms deviation of the Cα atoms of the current structure with the M344H-Gal-T1·UDP-Gal·Mn^{2+} structure is only 0.6 Å, indicating the binding of the acceptor substrate has not significantly changed the overall structure of the molecule (Figure 5a). Of the six coordinations seen for the Mn^{2+}, only five are quite similar to those found in the crystal structure of the M344H-Gal-T1·UDP-Gal·Mn^{2+} complex. The sixth coordination, with the anionic oxygen atom of the phosphate [P(β)], is quite different. This is mainly due to the difference in the binding of UDP-hexanolamine to the M344H-Gal-T1 molecule. Although the overall binding of the UDP-hexanolamine is quite similar to the binding of UDP to the wild-type β4Gal-T1 in the closed conformation, the hexanolamine moiety at the anionic oxygen atom of the phosphate group

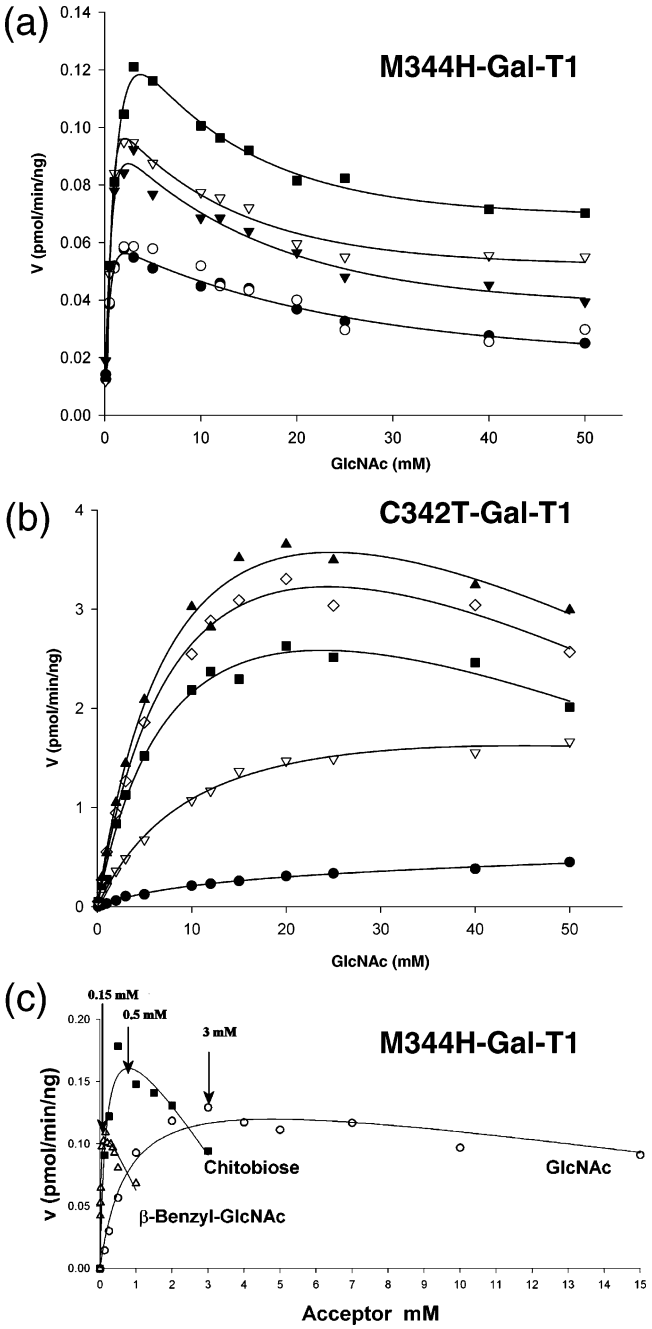

FIGURE 3: Effect of GlcNAc concentration on Gal-T activity of the M344H-Gal-T1 mutant (a) and wild-type enzyme, C342T-Gal-T1 (b), at different fixed concentrations of Mn^{2+}: (a) (●) 6 μM, (○) 20 μM, (▼) 0.5 mM, (▽) 1.5 mM, and (■) 5 mM and (b) (●) 6 μM, (▽) 80 μM, (■) 0.5 mM, (◇) 1.5 mM, and (▲) 5 mM. The activity of the mutant (a) is inhibited above 2−5 mM GlcNAc at any concentrations of Mn^{2+}, whereas the activity of the wild type (b) is inhibited at 25−30 mM GlcNAc and above 0.5 mM Mn^{2+}. (c) Effect of either GlcNAc, chitobiose, or β-benzyl-GlcNAc concentration on Gal-T activity of the mutant M344H-Gal-T1 in the presence of 5 mM Mn^{2+}. Arrows indicate the inhibition concentration for the respective curves. It is known that the disaccharide chitobiose binds strongly to the Gal-T1 compared to the monosaccharide GlcNAc. The higher the affinity of the acceptor substrate, the lower the required inhibition concentrations.

[P(β)] could not be accommodated inside the galactose binding pocket. Thus, the whole phosphate group is displaced from the catalytic pocket and placed above the Trp314 side chain (Figure 5b).

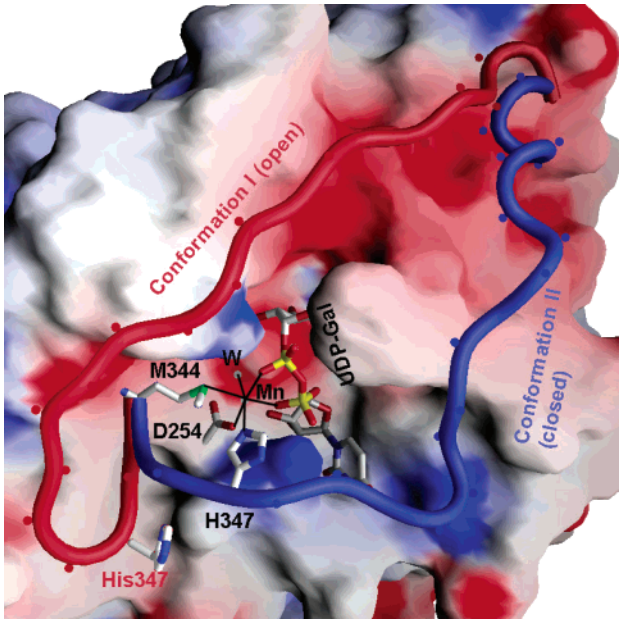

FIGURE 4: Comparison of the conformation of the long loop region of the open and closed structures of wild-type β4Gal-T1 (PDB entries 1FGX and 1O0R) (*6*, *11*, *13*). The electrostatic surface diagram of the portion of the enzyme molecule is shown, except for the long loop of residues 345−365. The negatively charged surface regions are red, while the positively charged surface regions are blue. The red tube corresponds to the open conformation of the long loop, while the blue tube corresponds to the closed conformation. In the open conformation, the long loop is placed in such a way that its His347 residue is away from the metal binding site. However, in the closed conformation (blue tube), the His residue forms a strong coordination bond with the metal ion. After catalysis, to release the product, UDP, and Mn^{2+}, the enzyme returns to the open conformation. At this stage, the Mn^{2+} is expected to have only two coordination bonds with the enzyme molecule: with residues Asp254 and Met344. Since the coordination bond with the Met344 residue is weak, the bound UDP and Mn^{2+} can be released efficiently.

The acceptor disaccharide molecule, chitobiose, can be clearly located from the difference Fourier electron density maps (Figure 5a). Binding of the acceptor sugar, GlcNAcβ1−4GlcNAc, is observed with β4Gal-T1 in the absence of LA for the first time, and the interactions of the nonreducing end GlcNAc moiety of chitobiose with the M344H-Gal-T1 molecule in the crystal structure presented here are quite similar to those found in the β4Gal-T1·LA·GlcNAc complex (*7*, *11*). The *N*-acetyl moiety of the GlcNAc molecule is bound in the hydrophobic pocket created by residues Arg359, Phe360, and Ile363. The side chain carboxylate group of Asp318 forms a hydrogen bond with the O4 hydroxyl group of the acceptor GlcNAc moiety of chitobiose (Figure 5c). Although the GlcNAc residue at the reducing end does not form any direct hydrogen bond with the M344H-Gal-T1 molecule, it forms hydrophobic interactions with the aromatic side chain of Tyr286 (Figure 5c). Enzyme kinetics studies have shown that at lower concentrations of GlcNAc the presence of LA enhances the transfer of Gal to GlcNAc; however, in the presence of chitobiose, LA exhibits competitive inhibition of the catalytic activity (*15*, *28*). In the crystal structure of the β4Gal-T1·LA·GlcNAc complex, the aromatic side chain of Phe31 of the LA molecule was found to interact with the Tyr286 side chain of the β4Gal-T1 molecule (*7*, *11*). Thus, LA competes for the same binding site (Tyr286) on β4Gal-T1 as the extended sugar residue of the chitobiose,

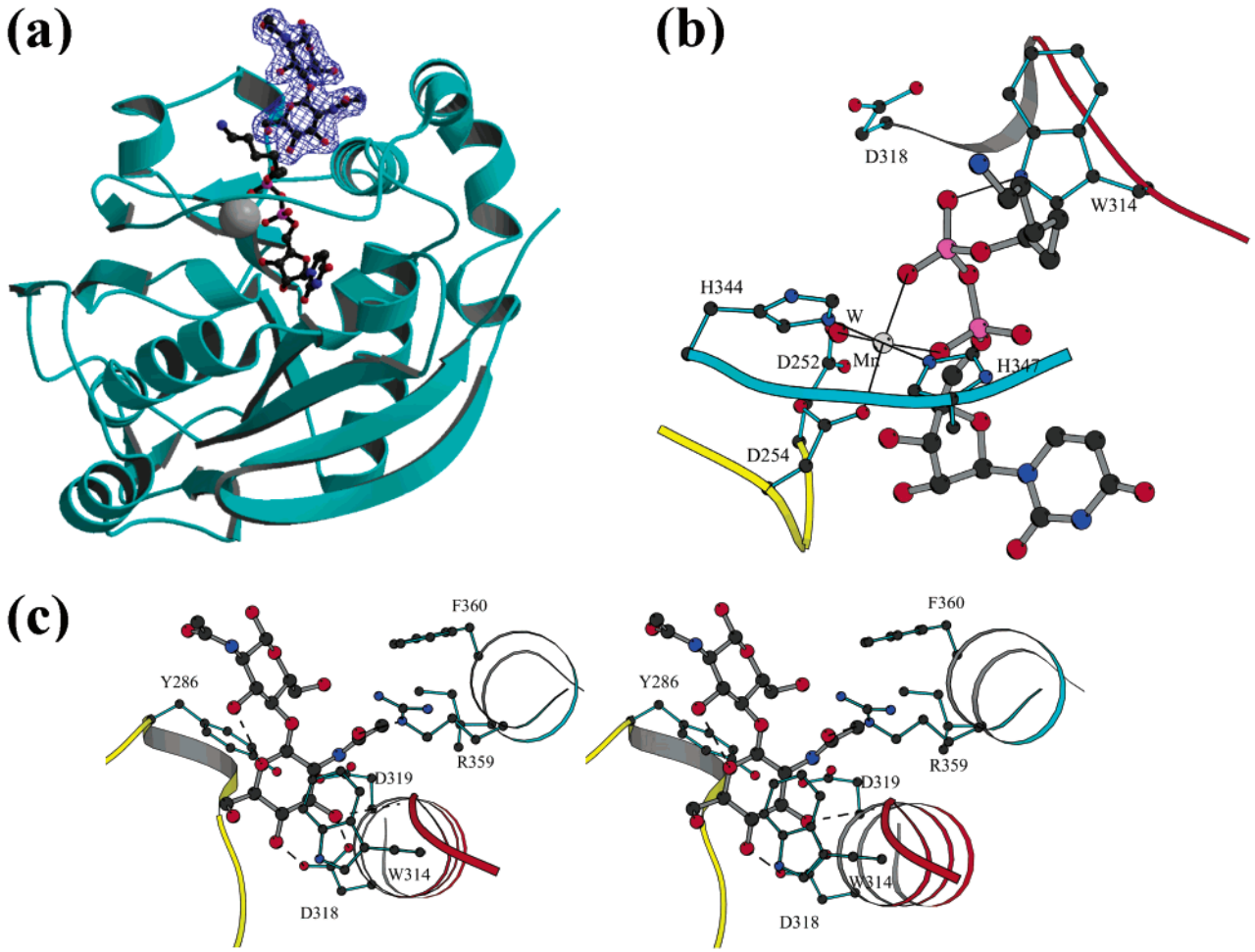

FIGURE 5: (a) Overall crystal structure of the M344H-Gal-T1 mutant in the presence of UDP-hexanolamine, Mn^{2+}, and chitobiose. The difference Fourier electron density map contoured at 3σ for the acceptor substrate is shown in blue. The Mn^{2+} is shown as a gray ball, while the UDP-hexanolamine is shown as a thick ball-and-stick diagram. (b) Molecular interactions of UDP-hexanolamine with the M344H-Gal-T1 molecule. Of the six coordinations found for the Mn^{2+}, the coordination with the P(β) phosphate anionic oxygen atom is different from those of the earlier crystal structures. This is due the presence of the hexanolamine moiety, which could not be accommodated inside the Gal binding site. (c) Stereodiagram of binding of chitobiose to the M344H-Gal-T1 mutant. As can be seen, the GlcNAc binding of the acceptor in the active site in this structure is quite similar to that observed in the β4Gal-T1·LA·GlcNAc complex. However, the nonreducing GlcNAc residue of chitobiose forms hydrophobic interactions with the Tyr286 side chain aromatic region. The conformational torsion angles, ϕ(O5−C1−O4−C4) and ψ(C1−O4−C4−C5), of the disaccharides are −77° and −130°, respectively, and they are similar to those of the β-chitin structure (*28*). Furthermore, as in the β-chitin structure, there is an intramolecular hydrogen bond observed between the O3 hydroxyl group and O5 of the chitobiose molecule.

an observation that is in accord with the kinetic data. These extra hydrophobic interactions alone seem to reduce the K_m value for chitobiose to 1 mM, compared to 5 mM for the monosaccharide, GlcNAc molecule. It is important to note that among the β4Gal-T1 family members, this Tyr286 residue is highly conserved. Since β4Gal-T1 is mainly involved in the synthesis of complex *N*-glycan structures, as predicted earlier, longer oligosaccharides are expected to utilize the predicted oligosaccharide binding site on β4Gal-T1 (*10*). However, β4Gal-T1 is also involved in the synthesis of short oligosaccharides attached to proteins such as core structures, and the structure presented here serves as a model for the binding of such sugars. Using this mutant, we have been successful in crystallizing the enzyme in complex with various higher oligosaccharides (unpublished work). These studies are expected to reveal the binding of the oligosaccharide to β4Gal-T1.

CONCLUSION

Results presented here show that in β4Gal-T1, the metal ion, in combination with a specific residue at position 344, plays an essential role in determining the k_{cat} of the enzyme. Metal ion, together with UDP-Gal, has two functions. First, it must induce a conformational change, and second, it must engage in the formation and stabilization of the transition state complex during catalysis. It is the combination of a Met residue at position 344 with Mn^{2+} or the His residue with Mg^{2+} that determines the high k_{cat} of the enzyme. The inability of the M344H-Gal-T1 mutant to return to the open conformation in the presence of UDP and Mn^{2+} has enabled us to crystallize the mutant in complex with chitobiose, a disaccharide acceptor, or with various higher oligosaccharides. The crystal structures of the complexes show that the second residue of the sugar acceptor forms an extensive hydrophobic interaction with the highly conserved Tyr286 residue of β4Gal-T1.

NOTE ADDED IN PROOF

Mutation of the corresponding Met344 residue in human and mouse β4Gal-T1 to His exhibits similar enzymatic and kinetic properties as presented with bovine β4Gal-T1.

ACKNOWLEDGMENT

We thank Dr. Alexander Wlodawer for the critical reading of the manuscript. We thank Dr. Zbigniew Dauter (National Cancer Institute, Brookhaven National Laboratory) for his help in data collection.

SUPPORTING INFORMATION AVAILABLE

Difference Fourier electron density maps for the metal-bound UDP-Gal in the crystal structure of both the Mn^{2+}- and Mg^{2+}-bound structures and final electron density maps contoured at 1σ for the substrates in the crystal structure of the M344H-GalT1·UDPH·Mn^{2+}·chitobiose complex. This material is available free of charge via the Internet at http://pubs.acs.org.

REFERENCES

1. Brew, K., Vanaman, T. C., and Hill, R. L. (1968) The role of α-lactalbumin and the A protein in lactose synthetase: a unique mechanism for the control of a biological reaction, *Proc. Natl. Acad. Sci. U.S.A. 59*, 491−497.
2. Takase, K., and Ebner, K. E. (1984) Interaction of galactosyltransferase with α-lactalbumin and substrates, *Curr. Top. Cell Regul. 24*, 51−62.
3. Powell, J. T., and Brew, K. (1976) Metal ion activation of galactosyltransferase, *J. Biol. Chem. 251*, 3645−3652.
4. Lo, N. W., Shaper, J. H., Pevsner, J., and Shaper, N. L. (1998) The expanding β4-galactosyltransferase gene family: messages from the databanks, *Glycobiology 8*, 517−526.
5. Amado, M., Almeida, R., Schwientek, T., and Clausen, H. (1998) Identification and characterization of large galactosyltransferase gene families: galactosyltransferases for all functions, *Biochim. Biophys. Acta 1473*, 35−53.
6. Gastinel, L. N., Cambillau, C., and Bourne, Y. (1999) Crystal structures of the bovine β4-galactosyltransferase catalytic domain and its complex with uridine diphosphogalactose, *EMBO J. 18*, 3546−3557.
7. Ramakrishnan, B., and Qasba, P. K. (2001) Crystal structure of lactose synthase reveals a large conformational change in its catalytic component, the β1,4-galactosyltransferase-I, *J. Mol. Biol. 310*, 205−218.
8. Ramakrishnan, B., Shah, P. S., and Qasba, P. K. (2001) α-Lactalbumin (LA) stimulates milk β-1,4-galactosyltransferase I (β4Gal-T1) to transfer glucose from UDP-glucose to *N*-acetylglucosamine. Crystal structure of β4Gal-T1·LA complex with UDP-Glc, *J. Biol. Chem. 276*, 37665−37671.
9. Ramakrishnan, B., and Qasba, P. K. (2002) Structure-based design of β1,4-galactosyltransferase I (β4Gal-T1) with equally efficient *N*-acetylgalactosaminyltransferase activity: point mutation broadens β4Gal-T1 donor specificity, *J. Biol. Chem. 277*, 20833−20839.
10. Ramakrishnan, B., Balaji, P. V., and Qasba, P. K. (2002) Crystal structure of β1,4-galactosyltransferase complex with UDP-Gal reveals an oligosaccharide acceptor binding site, *J. Mol. Biol. 318*, 491−502.
11. Ramakrishnan, B., and Qasba, P. K. (2003) Comparison of the closed conformation of the β1,4-galactosyltransferase-1 (β4Gal-T1) in the presence and absence of α-lactalbumin (LA), *J. Biomol. Struct. Dyn. 21*, 1−8.
12. Gunasekaran, K., Buyong, M., Ramakrishnan, B., Qasba, P. K., and Nussinov, R. (2003) Interdependence of backbone flexibility, residue conservation, and enzyme function: a case study on β1,4-galactosyltransferase-I, *Biochemistry 42*, 3674−3687.
13. Ramasamy, V., Ramakrishnan, B., Boeggeman, E., and Qasba, P. K. (2003) The role of tryptophan 314 in the conformational changes of β1,4-galactosyltransferase-I, *J. Mol. Biol. 331*, 1065−1076.
14. Brodbeck, U., Denton, W. L., Tanahashi, N., and Ebner, K. E. (1967) The isolation and identification of the B protein of lactose synthetase as α-lactalbumin, *J. Biol. Chem. 242*, 1391−1397.
15. Bell, J. E., Beyer, T. A., and Hill, R. (1976) The kinetic mechanism of bovine milk galactosyltransferase. The role of α-lactalbumin, *J. Biol. Chem. 251*, 3003−3013.
16. Powell, J. T., and Brew, K. (1976) A comparison of the interactions of galactosyltransferase with a glycoprotein substrate (ovalbumin) and with α-lactalbumin, *J. Biol. Chem. 251*, 3653−3663.
17. Geren, C. R., Magee, S. C., and Ebner, K. E. (1975) Circular dichroism changes in galactosyltransferase upon substrate binding, *Biochemistry 14*, 1461−1463.
18. Boeggeman, E., and Qasba, P. K. (2002) Studies on the metal binding sites in the catalytic domain of β1,4-galactosyltransferase, *Glycobiology 12*, 395−407.
19. Boeggeman, E., Balaji, P. V., Sethi, N., Masibay, A. S., and Qasba, P. K. (1993) Expression of deletion constructs of bovine β-1,4-galactosyltransferase in *Escherichia coli*: importance of Cys134 for its activity, *Protein Eng. 6*, 779−785.
20. Herbert, J. F. (1975) *Initial Rate Enzyme Kinetics*, Springer-Verlag, New York.
21. Otwinowski, Z., and Minor, W. (1997) Processing of X-ray diffraction data collected in oscillation mode, *Methods Enzymol. 276*, 307−326.
22. Brünger, A. T., Adams, P. D., Core, G. M., DeLano, W. L., Gros, P., Grosse-Kunstleve, R. W., Jiang, J. S., Kuszewski, J., Nilges, M., Pannu, N. S., Read, R. J., Rice, L. M., Simonson, T., and Warren, G. L. (1998) *Acta Crystallogr. D54*, 905−921.
23. Karulis, P. J. (1991) MOLSCRIPT: a program to produce both detailed and schematic plots of structures, *J. Appl. Crystallogr. 24*, 946−950.
24. Esnouf, R. M. (1999) Further additions to MolScript version 1.4, including reading and contouring of electron-density maps, *Acta Crystallogr. D55*, 938−940.
25. Nicholls, A., Sharp, K. A., and Honig, B. (1991) Protein folding and association: insights from the interfacial and thermodynamic properties of hydrocarbons, *Proteins 11*, 281−296.
26. Khatra, B. S., Herries, D. G., and Brew, K. (1974) Some kinetic properties of human-milk galactosyltransferase, *Eur. J. Biochem. 44*, 537−560.
27. Morrison, J. F., and Ebner, K. E. (1971) Studies on galactosyltransferase. Kinetic investigations with *N*-acetylglucosamine as the galactosyl group acceptor, *J. Biol. Chem. 246*, 3977−3984.
28. Grobler, J. A., Wang, M., Pike, A. C. W., and Brew, K. (1994) Study by Mutagenesis of the Roles of Two Aromatic Clusters of α-Lactalbumin in Aspects of Its Action in the Lactose Synthase System, *J. Biol. Chem. 269*, 5106−5114.
29. Gardner, K. H., and Blackwell, J. (1975) Refinement of β-chitin, *Biopolymers 14*, 1581−1595.

BI049007+